Submitted to the
**EPS HEP Conference**
**July 2003, Aachen**

**Abstract: 509** **Parallel Session(s): HQCD,HP**

# Observation of isolated high-$E_T$ photons in deep inelastic scattering

ZEUS Collaboration

**Abstract**

First measurements of cross sections for isolated prompt photon production in deep inelastic $ep$ scattering are presented for photon virtualities above $35\,\mathrm{GeV}^2$. The measurements were made with the ZEUS detector at HERA using an integrated luminosity of 121 $\mathrm{pb}^{-1}$. A signal for well-isolated photons in the transverse energy and pseudorapidity range $5 < E_T^\gamma < 10\,\mathrm{GeV}$, $-0.7 < \eta^\gamma < 0.9$ was observed, after the subtraction of the background from neutral mesons. Cross sections are presented for inclusive prompt photons and for those accompanied by one jet in the range $E_T^{\mathrm{jet}} \geq 6\,\mathrm{GeV}$, $-1.5 \leq \eta^{\mathrm{jet}} < 1.8$. Theoretical calculations made to $O(\alpha^2\alpha_S)$ describe reasonably well the measured photon plus jet cross sections.

# 1 Introduction

High transverse-momentum isolated final-state photons provide a direct probe of the dynamics of hard subprocesses in high energy collisions. These 'prompt' photons are observed without undergoing further interactions, thus accessing the parton-level processes with small hadronisation effects. Previous ZEUS measurements have studied the production of prompt photons in photoproduction processes [1–3]. Here, for the first time, prompt photon measurements in deep inelastic scattering (DIS) are reported, both inclusively and accompanied by jets. The measurement of prompt photons with jets allows a comparison with parton-level calculations.

Prompt photons are produced in lowest order QCD as shown in Fig. 1, or by radiation from the incoming or outgoing electron line. In addition, gluons can be radiated from the quark lines, or a final state with two high-$p_T$ objects can be formed by photon-gluon fusion. These processes have been calculated to order $O(\alpha^2\alpha_S)$ by Gehrmann-DeRidder, Kramer and Spiesberger [4], including interference terms for initial-state and final-state radiation from the electron line. By contrast, leading-logarithm parton-shower Monte Carlos do not naturally predict events with two hard scales ($Q^2$ and $E_T^\gamma$, the exchanged photon virtuality and the transverse energy of the emitted prompt photon).

Results are presented for the process $ep \to e\gamma X$, where $X$ is anything or is one jet within a defined rapidity and transverse energy range.

# 2 Apparatus and event selection

A data sample with an integrated luminosity of 121 pb$^{-1}$ was used, taken by the ZEUS detector between 1996 and 2000 and incorporating both $e^+p$ and $e^-p$ runs. The event sample corresponds to the sum of 38 pb$^{-1}$ of $e^+p$ data at a centre of mass energy of 300 GeV and 68 pb$^{-1}$ at 318 GeV, plus 16 pb$^{-1}$ of $e^-p$ data at 318 GeV. A single set of results is presented for this combined sample. Note that $e^+p$ and $e^-p$ differences are negligible after the acceptance cuts designed to minimise interference effects between photon emission from quark and from lepton lines. The Monte-Carlo cross sections (see section 4) differ by under 4% at the two energies. To gain statistical accuracy, the whole data sample was treated as a single unit.

A description of the ZEUS apparatus and luminosity monitor is given elsewhere [5]. Of particular importance in the present work are the uranium calorimeter (CAL) and the central tracking detector (CTD).

The CAL [6] has an angular coverage of 99.7% of $4\pi$ and is divided into three parts (FCAL, BCAL, RCAL), covering the angular ranges $2.6^\circ - 36.7^\circ$, $36.7^\circ - 129.1^\circ$ and $129.1^\circ - 176.2^\circ$

respectively.[1]

Each part consists of towers longitudinally subdivided into electromagnetic (EMC) and hadronic (HAC) cells. The electromagnetic section of the BCAL (BEMC) consists of cells of 20 cm length azimuthally and mean width 5.45 cm in the $Z$ direction at a mean radius of 1.3 m from the beam line. These cells have a projective geometry as viewed from the interaction point. The profile of the electromagnetic signals observed in clusters of cells in the BEMC provides a partial discrimination between those originating from photons or positrons, and those originating from neutral meson decays.

The CTD [7] is a cylindrical drift chamber situated inside a superconducting solenoid which produces a 1.43 T field. Using the tracking information from the CTD, the vertex of an event can be reconstructed with a resolution of 0.4 cm in $Z$ and 0.1 cm in $X, Y$. In this analysis, the CTD tracks are used to reconstruct the event vertex, and also in the selection criteria for high-$E_T$ photons.

The event trigger used selected DIS events with an observed scattered electron.

Offline, events were first selected which pass DIS cuts in ZEUS, similar to those used in previous analyses, [8] with exchanged photon virtuality $Q^2$ as reconstructed from the final-state electron above 35 GeV$^2$, and have a suitable photon candidate present. The scattered electron (or positron) energy is required to be above 10 GeV and its direction is required to be in the range 139.8° to 171.9°, in order to be well measured in the RCAL and far from the photon.

In order to be selected, events were required to have a reconstructed vertex position $-40 < Z_{\rm vtx} < 40$ cm, and to select well reconstructed DIS events $35 < E - p_z < 65\,{\rm GeV}$, $y_{\rm el} < 0.70$ and $y_{\rm jb} > 0.04$ where $y_{\rm el}$ is the Bjorken scaling variable reconstructed using information on the outgoing electron and $y_{\rm jb} = \Sigma(E - p_z)/2E_e$.

# 3 Photon candidate selection

The identification of events containing an isolated prompt photon candidate follows closely the approach used for the measurement of prompt photon candidates in photoproduction at HERA [1]. Events are selected on the basis of an isolated photon candidate detected in the BCAL, where the background subtraction using calorimeter cells is well understood. The photon algorithm selected predominantly electromagnetic clusters of cells within a

[1] The ZEUS coordinate system is right-handed with positive-$Z$ in the proton beam direction and an upward-pointing $Y$ axis. The nominal interaction point is at $X = Y = Z = 0$.. All kinematic quantities are given in the laboratory frame. Pseudorapidity $\eta$ is defined as $-\ln(\tan(\theta/2))$, where $\theta$ is the polar angle relative to the $Z$ direction, measured from the $Z$ position of the event vertex.

small angular cone, and accepts larger electromagnetic clusters than are typical of a single photon. Use of shower shapes as a discriminant, (as described below,) allows subtraction of the background from $\pi^0$ and $\eta$ production.

Cuts were applied to the photon candidate to define its kinematics and restrict it to the BCAL; it was required that the reconstructed transverse energy of the cluster $E_T^\gamma > 5\,\mathrm{GeV}$, and the pseudorapidity using the reconstructed vertex $-0.7 < \eta^\gamma < 0.9$. A cut $E_T^\gamma < 10\,\mathrm{GeV}$ was imposed in order for the $\pi^0$ and $\eta$ subtraction method to be effective.

In addition the photon-candidate cluster should be isolated from all other activity. The isolation is defined in terms of $\Delta r$, where $\Delta r^2 = \Delta\phi^2 + \Delta\eta^2$, the distance to the nearest reconstructed track in $\eta - \phi$ space, $\Delta r > 0.2$. Within a cone in $\eta - \phi$ of radius 1.0 around the photon candidate, the ratio $E_T^\gamma / E_T^{\mathrm{cone}}$ displays a continuum with a strong peak at 1.0 corresponding to isolated photon candidates. It was demanded that $E_T^\gamma / E_T^{\mathrm{cone}} > 0.9$.

The photon is thus well separated from the electron to minimise the contribution from initial-state and final-state photon radiation (ISR and FSR), where the photon is usually produced at a small angle to the parent lepton. Studies based on DJANGOH [9–11] show that, for electrons in the range defined in section 2 above, photons radiated from the lepton lines essentially always fall outside the photon acceptance used in this analysis.

The energy isolation cone suppresses the contribution from photon candidates produced within jets. A cut was made to remove deeply virtual Compton scattering (DVCS) by demanding at least two tracks reconstructed in the CTD. (In DVCS the final state seen in the detector is a photon plus a well-separated electron only).

Studies based on single-particle Monte Carlo samples showed that the photon energy measured in the BCAL was on average less than the true value, owing to the dead material in front of the BCAL. To compensate for this, an energy correction, typically 0.2 GeV, was added. [3].

The above selection of events still includes a sizeable contribution from neutral mesons, such as $(\pi^0, \eta)$, which decay to photons. The single-photon signal was statistically extracted from the background using BCAL energy cluster shapes. First we look at $\langle \delta Z \rangle$ where $\langle \delta Z \rangle = \Sigma(E_{\mathrm{cell}} | Z_{\mathrm{cell}} - \overline{Z}|)/\Sigma E_{\mathrm{cell}}$. Here $Z$ counts the BCAL cell number along the beam direction. Fig. 2 shows the distribution for data, together with a fit based on photon shower shapes plus simulation of single particles in the detector,($\pi^0$ and $\eta$). The photon shower shapes used were derived in two ways. In Fig 2. these are for photons found in DVCS data events. Single photon Monte Carlo shower shapes were used as an alternative, and the sensitivity of the background subtraction to distortions of the shape was investigated as part of the systematic error study. The results of the two methods give indistinguishable background subtractions but differ in an overall scale factor by 5% on the prompt photon signal acceptance. Because of the higher statistics available in MC,

allowing rapidity and energy dependences of shower shapes to be modelled, this method was used in the analysis.

Events with $\langle \delta Z \rangle < 0.65$ were retained, and the fit to the higher $\langle \delta Z \rangle$ range was used to determine the $\eta$ fraction to be taken in a subsequent fit to $f_{\max}$, which is the ratio of the energy of the highest energy cell in an electromagnetic cluster to the total cluster energy. When incident on the BCAL, single photons form narrow clusters, with most of the energy going into only one cell, giving an $f_{\max}$ distribution peaked close to unity. In contrast, the neutral mesons decay to more than one photon forming a larger cluster in the calorimeter. The distributions for $\pi^0$ and $\eta$ were modelled using single particle Monte Carlo as done in the photoproduction analysis. [1]

Deeply Virtual Compton Scattering (DVCS) data and single-particle Monte Carlo simulation show that most of the prompt photon signal is at $f_{\max} > 0.75$. The prompt photon signal and background are extracted from the fit of the Monte Carlo to the $\langle \delta Z \rangle$ and $f_{\max}$ distributions, done separately for each bin in each plot presented below. 1875 events survive with $\langle \delta Z \rangle < 0.65$ of which 877 have $f_{\max} > 0.75$, yielding a signal of 572 and background of 1303 events, as extracted using the fitting method described previously. [1]

# 4 Monte Carlo event simulation

The Monte Carlo (MC) programs PYTHIA 6.206 [12] and HERWIG 6.1 [13], were used to simulate prompt photon emission for the study of event reconstruction efficiency. Both programs make predictions that are in different ways at variance with our results in some distributions. The data acceptances evaluated using PYTHIA and HERWIG are in general very similar.

In both generators, the partonic processes are simulated using leading-order matrix elements, with the inclusion of initial- and final-state parton showers. Fragmentation into hadrons is performed using the LUND [14] string model as implemented in JETSET [15] in the case of PYTHIA, and a cluster model [16] in the case of HERWIG. The events generated using the PYTHIA and HERWIG programs were used for calculating jet-energy corrections and correcting for detector and acceptance effects. The corrections provided by PYTHIA were used as default values and those given by HERWIG were used to estimate the systematic uncertainties coming from the treatment of the event dynamics and of parton shower and hadronisation. In general, the differences between the PYTHIA and HERWIG predictions for event energy corrections and for data acceptances were smaller than the statistical errors. There is a significant difference in acceptance affecting jet rapidity due to different photon-jet correlations and the impact of the photon isolation cut. This is taken into account in the systematic error.

All generated events were passed through the ZEUS detector and trigger simulation programs based on GEANT 3.13 [17]. They were reconstructed and analysed by the same program chain as the data. The jet search was performed using the energy measured in the CAL cells in the same way as for the data, as described below. The same jet algorithm was also applied to the final-state particles.

# 5 Results

## 5.1 $ep \to e\gamma + X$

The cross sections were measured using the selected inclusive sample of prompt photon events. The results are given in Fig. 3. The systematic errors considered were as follows: variations around the nominal $f_{max}$ spectra for photon and $\pi^0$ affecting the signal extraction, change in the detector energy scale calibration by $\pm 3\%$, reflecting the overall energy scale uncertainty, and change in the energy scale in both Monte Carlo and data by $\pm 10\%$ for photons. This last figure is motivated by the r.m.s. differences between hadron-level generated and reconstructed energies. (The means have been adjusted to agree to better than 1% as part of the calibration procedure.) Also included as a systematic error is the difference between HERWIG and PYTHIA (mostly well below the statistical error.) Not included in the figures is a (+5-7%) systematic uncertainty in cross-section arising from differences in photon shower shape between DVCS data and single-particle Monte Carlo.

A clear signal for isolated prompt photon emission in DIS is seen, peaked at low values of pseudorapidity. The measured cross-section is quoted for the following cuts: $Q^2 > 35$ GeV$^2$, $y_{el} < 0.7$, $E_e > 10$ GeV, $139.8^\circ < \theta_e < 171.8^\circ$, $-0.7 < \eta_\gamma < 0.9$, $5 < E_T^\gamma < 10$ GeV, photon isolation such that at least 90% of the energy found in a cone of $\Delta r = 1.0$ around the photon is associated directly with the photon. The result found, including all systematic errors, is

$$\sigma(ep \to e\gamma X) = (5.64 \pm 0.58(\text{stat.})^{+0.33}_{-0.82}(\text{syst.}))\ \text{pb}$$

For these events we find the mean values of $Q^2$ and $x_{\text{Bj}}$ are $87\,\text{GeV}^2$ and 0.0049. For the Monte Carlo simulations using the same acceptance cuts as the data the values obtained were $87\,\text{GeV}^2$ and 0.0047 for PYTHIA and $62\,\text{GeV}^2$ and 0.0017 for HERWIG. The HERWIG photon rapidity distribution peaks at low $\eta$ like the data, whereas for PYTHIA the peak is in the forward direction. The cross-sections predicted by PYTHIA and HERWIG are low compared to the data by factors of about 3 and 9 respectively. Thus neither generator resembles the data well.

## 5.2 $ep \to e\gamma + \text{jet} + \text{X}$

At the parton level, prompt photons are emitted from fermion lines. To enable a comparison to be made to QCD predictions we therefore look for jets accompanying the prompt photons.

Jets were reconstructed from calorimeter energy deposits using a cone algorithm with radius $\Delta r = 0.7$, ('EUCELL' algorithm [18]). Corrections to jet energies were evaluated using Monte Carlo simulated events, and are typically +(10-15)% for jets with measured energy above 6 GeV [3].

Jets are counted only if they have $E_T^{\text{jet}} > 6\,\text{GeV}$ and $-1.5 < \eta^{\text{jet}} < 1.8$. Fig. 4 shows the cross sections for photon plus one jet in the acceptance. An additional systematic error was considered of a change in the energy scale of both data and reconstructed Monte Carlo of ±20%, representing the r.m.s. differences between hadron-level and reconstructed jet energies. The measured total cross-section within these cuts for photon plus one jet, including all systematic errors, is

$$\sigma(ep \to e\gamma + \text{jet}) = (0.86 \pm 0.14(\text{stat.})^{+0.19}_{-0.13}(\text{syst.}))\ \text{pb}$$

The histograms on Fig. 4 show Monte Carlo predictions. We see that the transverse energies of photon and jet are described well. In HERWIG the photon rapidity is described well but the jet rapidity peaks at lower values, consistent with coming from lower $x_{\text{Bj}}$. In PYTHIA the jet rapidity is described well, but the photon rapidity peaks too far forward, as seen already in the inclusive photon case.

Figure 5 shows the same data with NLO ($O(\alpha^2\alpha_s)$) calculations superimposed. The boxed bands on the graphs represent predictions of Kramer and Spiesberger [19], following the approach they published earlier [4]. They chose as their renormalisation scale the transverse momentum of the jet. The band width shows the effect of changing this scale up or down by a factor of two. For (photon + jet) their calculation is next to leading order, so that the comparison to data is meaningful. They predict a total cross-section within the cuts stated above for the mixture of energies and beam charges used in this analysis of (1.33 ± 0.07) pb where the error corresponds to the change in the result when the renormalisation scale is changed as above. This is slightly above (1.7 S.D.) our measurement.

The agreement on the shape of distributions is mostly reasonable. Note that the theoretical calculation predicts more jets at forward rapidity, and at higher $E_T$ (beyond the boundary of figure 4(d)) than is seen in the data. For our acceptance their calculation predicts the mean value of $Q^2$ to be $118\,\text{GeV}^2$, in reasonable agreement with the data value of $(107 \pm 6)\,\text{GeV}^2$. However, they predict the mean value of $x_{\text{Bj}}$ to be 0.013, significantly above our data value of $(0.0041 \pm 0.0003)$.

# 6 Conclusion

First observations of prompt photon emission in deep inelastic scattering have been presented, together with distributions for accompanying jets. The event simulations used (PYTHIA and HERWIG) are each able to describe some but not all of the features of the data: cross-section, mean $Q^2$, mean $x_{Bj}$, photon and jet rapidity and transverse energy distributions.

The results have been compared to an $O(\alpha^2\alpha_S)$ calculation for $e + p \to e + \gamma + \text{jet}$. The level of agreement is mostly satisfactory in normalisation and shape for photon and jet rapidity and transverse energy distributions.

# 7 Acknowledgements

It is a pleasure to thank the DESY directorate and staff for their unfailing support in delivering high luminosity over the five year period for which data are used in this analysis. We have also benefitted greatly from conversations and assistance from G. Ingelman and T. Sjostrand, and particularly from G. Kramer and H. Spiesberger.

# References


[1] ZEUS Collaboration, J. Breitweg et al., Phys. Lett. B 413 (1997) 201.

[2] ZEUS Collaboration, J. Breitweg et al., Phys. Lett. B 472 (2000) 175.

[3] ZEUS Collaboration, S. Chekanov et al., Phys. Lett. B 511 (2001) 19.

[4] A. Gehrmann-De Ridder, G. Kramer and H. Spiesberger, Nucl. Phys. B 578 (2000) 326.

[5] ZEUS Collaboration, M. Derrick et al., Phys. Lett. B 297 (1992) 404.

[6] M. Derrick et al., Nucl. Inst. Meth. A 309 (1991) 77;
A. Andresen et al., Nucl. Inst. Meth. A 309 (1991) 101;
A. Caldwell et al., Nucl. Inst. Meth. A 321 (1992) 356;
A. Bernstein et al., Nucl. Inst. Meth. A 336 (1993) 23.

[7] N. Harnew et al., Nucl. Inst. Meth. A 279 (1989) 290;
B. Foster et al., Nucl. Phys. Proc. Suppl. B 32 (1993) 181;
B. Foster et al., Nucl. Inst. Meth. A 338 (1994) 254.

[8] ZEUS Collaboration, S. Chekanov et al., Eur. Phys. J. C 21 (2001) 443.

[9] K. Charchula, G.A. Schuler and H. Spiesberger, Comp. Phys. Comm. 81 (1994) 381.

[10] A. Kwiatkowski, H. Spiesberger and H.-J. Möhring, Comp. Phys. Comm. 69 (1992) 155. Also in *Proc. Workshop Physics at HERA*, 1991, DESY, Hamburg.

[11] G. Ingelman, A. Edin and J. Rathsman, Comp. Phys. Comm. 101 (1997) 108.

[12] T. Sjöstrand, Comp. Phys. Comm. 82 (1994) 74.

[13] G. Marchesini et al., Comp. Phys. Comm. 67 (1992) 465.

[14] B. Andersson et al., Phys. Rep. 97 (1983) 31.

[15] T. Sjöstrand, Comp. Phys. Comm. 39 (1986) 347;
T. Sjöstrand and M. Bengtsson, Comp. Phys. Comm. 43 (1987) 367.

[16] B. R. Webber, Nucl. Phys. B 238 (1984) 492.

[17] R. Brun et al., GEANT3, Technical Report CERN-DD/EE/84-1, CERN, 1987.

[18] ZEUS Collaboration, J. Breitweg et al., Eur. Phys. J. C 1 (1998) 109.

[19] G. Kramer and H. Spiesberger, private communication, 2002.

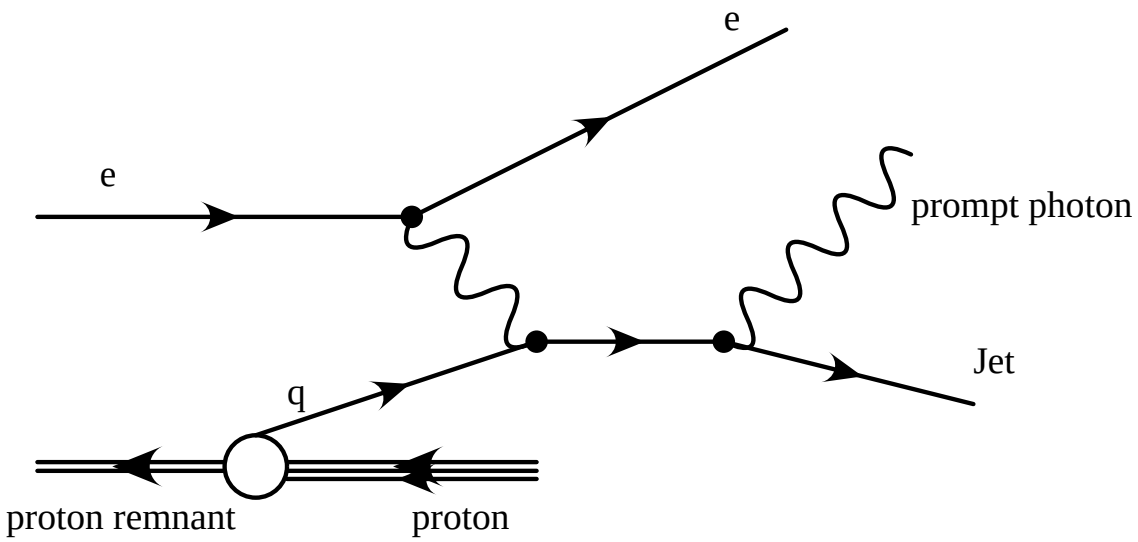


**Figure 1:** *Lowest-order prompt photon production in ep scattering.*

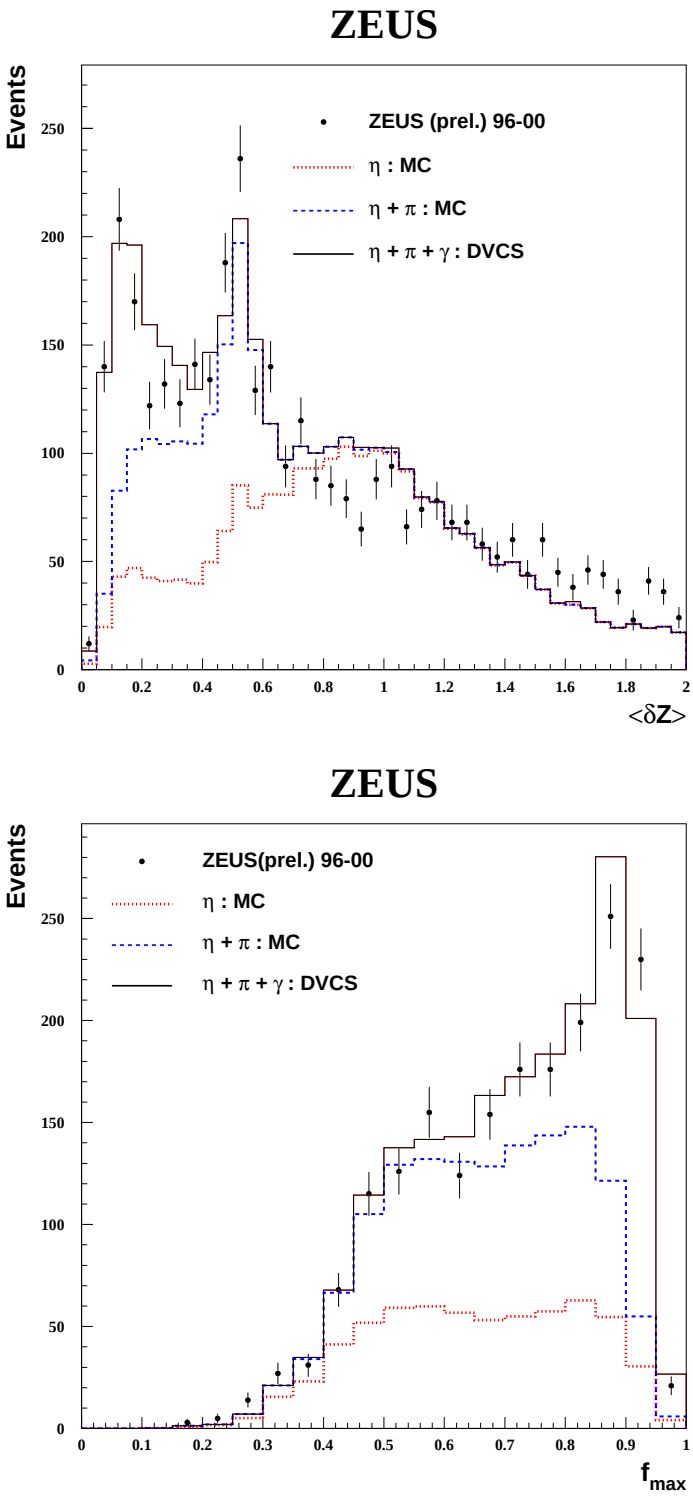


**Figure 2:** *Distribution of $\delta Z$ for prompt photon candidates in selected events. distribution of $f_{\max}$ after a cut on $\delta Z < 0.65$. Also given are fitted distributions for DVCS data $\gamma$ and Monte Carlo $\pi^0$ and $\eta$ mesons with similar selection criteria to the observed candidates.*

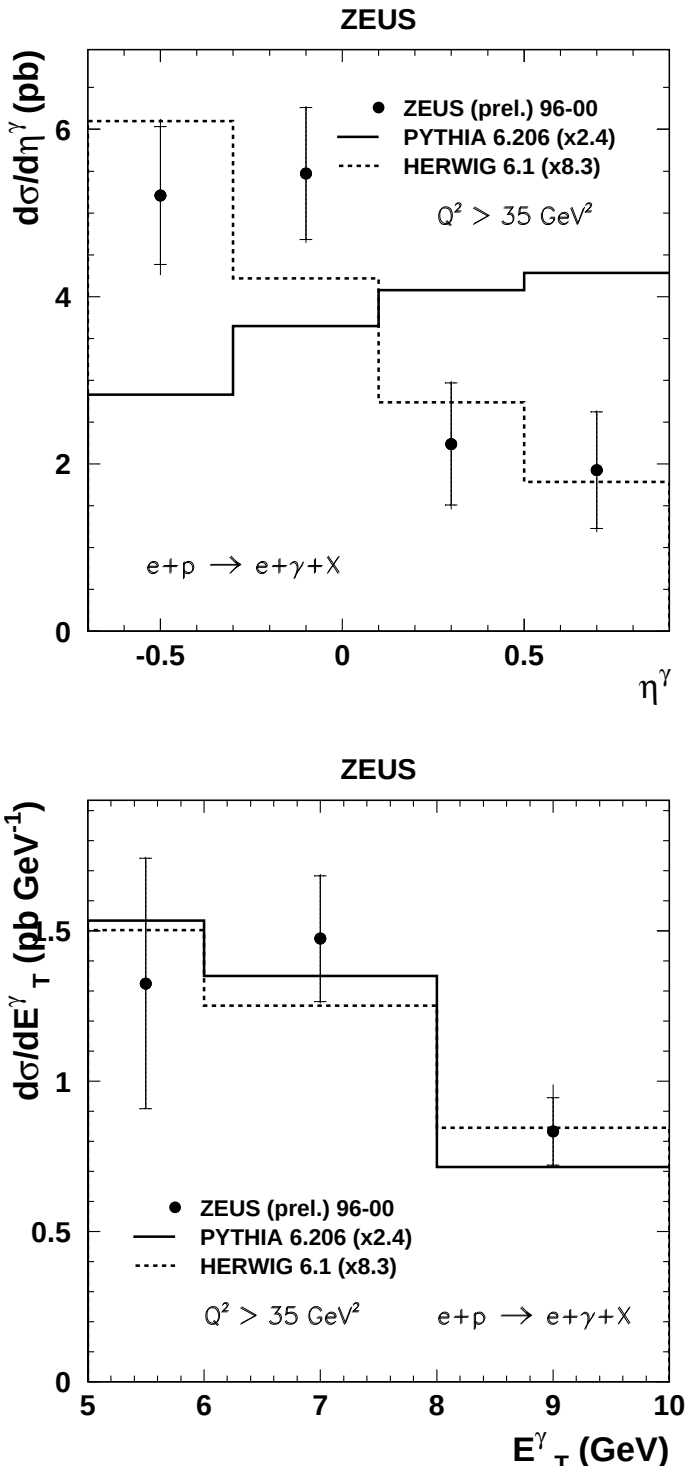


**Figure 3:** *Inclusive prompt photon cross section (a) rapidity,* $\mathrm{d}\sigma/\mathrm{d}\eta$ (pb) *(b) transverse energy* $\mathrm{d}\sigma/\mathrm{d}p_T$ (pb/GeV) *in the range* $-0.7 < \eta < 0.9$ *and* $5 < E_T < 10\,GeV$. *Inner error bars are statistical and the outer errors include systematic errors added in quadrature. Scale factor* $(0.95^{+0.05}_{-0.07})$ *due to shower shape not shown. The histograms show MC predictions, rescaled to data.*

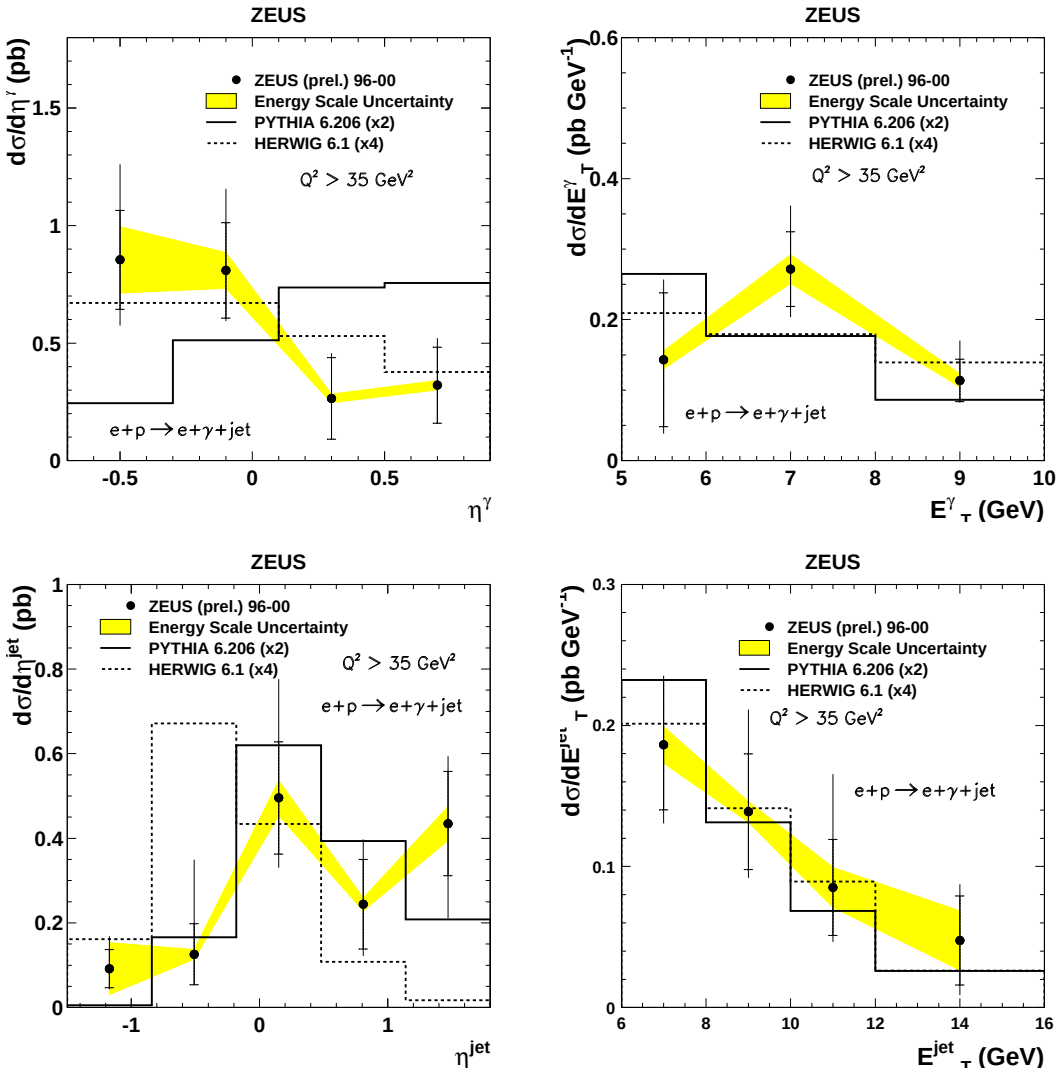


**Figure 4:** *Prompt photon plus jet cross section (a) photon rapidity,* $\mathrm{d}\sigma/\mathrm{d}\eta$ (pb) *(b) photon transverse energy* $\mathrm{d}\sigma/\mathrm{d}p_T$ (pb/GeV) *(c) jet rapidity,* $\mathrm{d}\sigma/\mathrm{d}\eta^{\mathrm{jet}}$ (pb) *(d) jet transverse energy* $\mathrm{d}\sigma/\mathrm{d}p_T^{\mathrm{jet}}$ (pb/GeV) *for events with a photon in the range* $-0.7 < \eta < 0.9$ *and* $5 < E_T < 10\,GeV$ *and one jet in the range* $-1.5 < \eta^{\mathrm{jet}} < 1.8$ *and* $E_T^{\mathrm{jet}} > 6\,GeV$*. Inner error bars are statistical and the outer errors represent systematic errors added in quadrature. The band around the data points shows the effect of energy scale uncertainty. Scale factor* $(0.95^{+0.05}_{-0.07})$ *due to shower shape not shown. The histograms show Monte Carlo predictions, normalised to the data.*

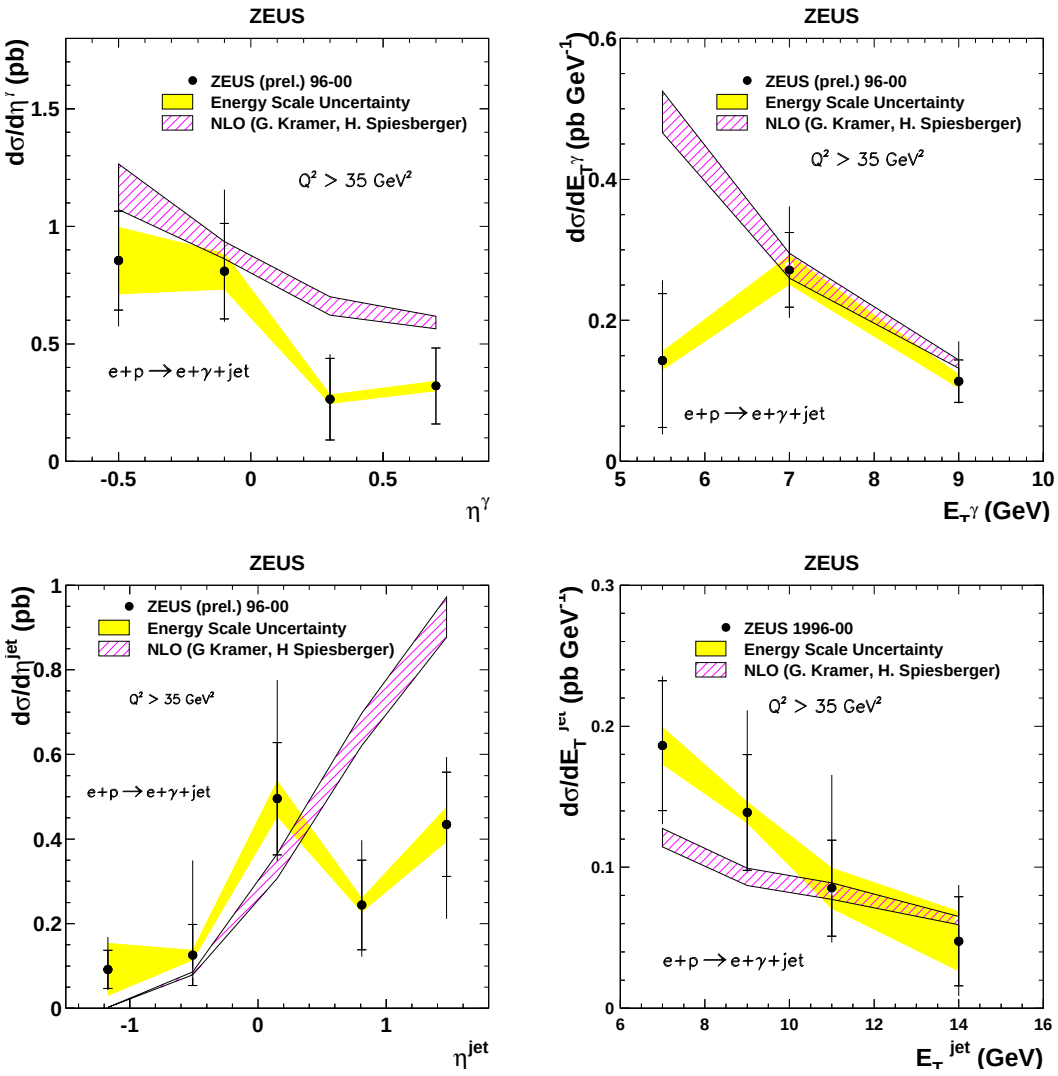


**Figure 5:** *Prompt photon plus jet cross section (a) photon rapidity,* $\mathrm{d}\sigma/\mathrm{d}\eta$ (pb) *(b) photon transverse energy* $\mathrm{d}\sigma/\mathrm{d}p_T$ (pb/GeV) *(c) jet rapidity,* $\mathrm{d}\sigma/\mathrm{d}\eta^{\mathrm{jet}}$ (pb) *(d) jet transverse energy* $\mathrm{d}\sigma/\mathrm{d}p_T^{\mathrm{jet}}$ (pb/GeV) *for events with a photon in the range* $-0.7 < \eta < 0.9$ *and* $5 < E_T < 10\,GeV$ *and one jet in the range* $-1.5 < \eta^{\mathrm{jet}} < 1.8$ *and* $E_T^{\mathrm{jet}} > 6\,GeV$*. Inner error bars are statistical and the outer errors represent systematic errors added in quadrature. The band around the data points shows the effect of energy scale uncertainty. Scale factor* $(0.95^{+0.05}_{-0.07})$ *due to shower shape not shown. The boxed band shows the predictions of Kramer and Spiesberger including the effect of renormalisation scale uncertainty.*